

A Study of Line Shape of CO Infrared Emission Lines*

James A. Dowling,** Shirleigh Silverman, William S. Benedict,*** and Jarus W. Quinn****

Office of the Associate Director, National Bureau of Standards, Washington, D.C. 20234

(March 2, 1971)

The shape of several vibration-rotation lines of CO emitted by a C₂H₂-O₂ flame was investigated. An equivalent width measurement was made using an absorption cell of room temperature CO as an analyzer. Analysis of the data showed that line shapes could be fitted to a Voigt function with shape parameters a between 1.0 and 1.5.

The collision widths of the flame lines, as determined by the shape parameters, are in essential agreement with earlier room temperature measurements. The extrapolation of the widths measured at room temperature to high temperature has been shown to be reliable within the uncertainty of this experiment ($\pm 15\%$).

Key words: Carbon monoxide; collision parameters; equivalent width; flame spectra; line shapes.

1. Introduction

The purpose of this work was to measure the line-broadening parameters in the fundamental band of CO, as emitted in a C₂H₂-O₂ flame. The two necessary parameters are the line strength and line shape. The line strength may be calculated for any temperature from a measurement of the lifetime or transition probability. At low pressures the line shape is determined by the Doppler effect and is a known factor of temperature and molecular mass. At high pressures the line shape is Lorentzian and is determined by the intermolecular forces as expressed by a collision-broadening diameter. Most measurements of this quantity have been made in a narrow temperature range near room temperature and the extrapolation to higher temperature is quite uncertain. For gases in the temperature range 1500 to 3500 K and the pressure range 0–1 atm the shape results from both Doppler and Lorentz broadening and is described by the Voigt function [1].

The spectral absorption coefficient for a line of resonant wavenumber ν_{u1} with a Voigt profile is:

$$P_\nu(\nu - \nu_{u1}, a) = P' \cdot V(\nu - \nu_{u1}, a) \quad (1)$$

where

$$a = \sqrt{\ln 2} \frac{\gamma_c}{\gamma_D} \quad (2)$$

$$P' = \frac{S}{\gamma_D} \sqrt{\frac{\ln 2}{\pi}} \quad (3)$$

γ is the collision half-width and γ_D is the Doppler half-width of the line, and the Voigt function $V(\nu - \nu_{u1}, a)$ is given by:

$$V(\nu - \nu_{u1}, a) = \frac{a}{\pi} \int_{-\infty}^{\infty} \frac{\exp(-y^2)}{a^2 + (x-y)^2} dy \quad (4)$$

$$\text{with } y = (\nu' - \nu_{u1}) \frac{\sqrt{\ln 2}}{\gamma_D}$$

$$\text{and } x = (\nu - \nu_{u1}) \frac{\sqrt{\ln 2}}{\gamma_D}.$$

The total absorption coefficient in the case of Voigt line shape is then given by:

$$P_\nu(\nu - \nu_{u1}, a) \cdot X = P' \cdot X \cdot V(\nu - \nu_{u1}, a) \quad (5)$$

where X is the optical density in appropriate units.

*This work was supported by the Air Force Cambridge Research Laboratories and is based on a thesis submitted (by J. A. Dowling) to the Physics Dept., Catholic University in partial fulfillment of the requirements for the degree of Doctor of philosophy. A preliminary account of this work was presented at the meeting of the Optical Society of America, Washington, D.C., March 1968.

**Present address: Naval Research Laboratory, Washington, D.C. 20390.

***Present address: Institute for Molecular Physics, The University of Maryland, College Park, Maryland 20740.

****Present address: Optical Society of America, 2100 Pennsylvania Ave., NW., Washington, D.C. 20037.

The parameter a determines the line shape for cases intermediate between the limiting behavior of a Doppler shape with $a=0$ and a shape that is essentially Lorentzian or collision broadened when $a \geq 10$.

The Doppler half-width γ_D is given by:

$$\gamma_D = 3.58 \times 10^{-7} \sqrt{T/M} \nu_{ul} \text{ cm}^{-1}$$

with T in Kelvin, M , the molecular weight in g/mol, and ν_{ul} in cm^{-1} .

For CO at 2143 cm^{-1} , γ_D is $2.40 \times 10^{-3} \text{ cm}^{-1}$ at 273.15 K and $8.58 \times 10^{-3} \text{ cm}^{-1}$ at 3500 K.

A simplified expression for the collision width γ_c is given by

$$\gamma_D = \frac{3.37 \times 10^{10}}{\pi c} \times \sigma_1 \sigma_2 \sqrt{\frac{M_1 + M_2}{M_1 M_2}} \times P / \sqrt{T} \text{ cm}^{-1} \quad (6)$$

where σ_1 , σ_2 , and M_1 , M_2 are the colliding molecular diameters in \AA , and molecular weights in grams per mol, respectively, and P is pressure in atmospheres. For self broadening [2] $\sigma_1 = \sigma_2 = 3.12 \text{ \AA}$, γ_c for CO is $5.63 \times 10^{-2} \text{ cm}^{-1}$ at 273 K and is $1.57 \times 10^{-2} \text{ cm}^{-1}$ at 3500 K and 1 atm. On this basis, referring to eq (2), the emission lines of CO in the vicinity of 2200 cm^{-1} should be described by Voigt profiles with $1 < a < 2$, for a pressure of 1 atm and temperature of 3500 K.

The effect of the finite bandpass of an observing instrument on the apparent shape and width of an observed spectral line has been treated elsewhere [3-6].

Kostkowski and Bass [5] give results of errors made in measured peak absorptions and line-widths. Their results show that accurate corrections may be applied to observed shapes for slit functions having widths a maximum of 1/2 to 1 times the half-width of the line under investigation. However, such a procedure for determining the actual line shape from the observed profile is not applicable in the present experiment.

The grating instrument used in the present experiment has a theoretical resolution of 0.04 to 0.05 cm^{-1} which is about three times greater than the anticipated line half-width. Therefore, one may resort to the curve-of-growth method which is implemented by changing the physical path length in order to change the optical path, maintaining a constant gas pressure, and thus, a constant value of γ_c . However, such a procedure is not readily adaptable to flame studies. Although the optical density can be varied by changing the pressure of the gas surrounding the flame, this would not allow observation of the lines at constant pressure, i.e., constant collision width. An alternative is to study several flames of various thicknesses.

The method described here employs an equivalent width measurement, but unlike a curve-of-growth procedure, the conditions in the flame remain fixed for a series of observations. An absorption cell containing CO is introduced between the flame source and the detector. The equivalent width in emission of a single line in the flame is measured with the cell evacuated.

Then known pressures of room temperature CO are sequentially admitted to the cell. The line is scanned at each absorber pressure, and a measurement is made of the net equivalent width which becomes progressively smaller with increasing pressure.

The equivalent width in emission (integrated emission) is:

$$R = R^\circ \int_{\Delta\nu} \epsilon(\nu) d\nu = R^\circ \int_{\Delta\nu} [1 - \exp(-P_\nu X)] d\nu \quad (7)$$

where R° , the blackbody radiance, is assumed to be constant over the small frequency range $\Delta\nu$.

The value of the integral is the integrated emissivity of the line. This quantity is observed experimentally when the absorption cell is evacuated. When CO is introduced into the absorption cell, the resultant observed emission $R^*(\nu)$ is:

$$R^*(\nu) = R^\circ [1 - \exp(-P_E X_E)] \exp(-P_A X_A) \quad (8)$$

where the subscripts E and A refer to the emitter and absorber respectively. If $R^*(\nu)$ is scanned by the spectrometer slit and the area under the observed record measured, we obtain the observed integrated emission:

$$R^* = \int_{\Delta\nu} R^*(\nu) d\nu \quad (9)$$

$$= R^\circ \int [1 - \exp(-P_{E\nu} \cdot X_E)] \exp(-P_{A\nu} \cdot X_A) d\nu.$$

The total absorption coefficient can be written

$$P_{E\nu} \cdot X_E = P'_E \cdot V_E(\nu, a_E) \cdot X_E \quad (10)$$

where $V_E(\nu, a_E)$ is the Voigt function describing the emission line. A similar relation holds for the Voigt function for the absorption line $V_A(\nu, a_A)$. However, a measurement of R^* does not determine the line shape parameter a_E uniquely in $V_E(\nu, a_E)$ since P'_E and a_E are both undetermined. However, one can make a unique determination by plotting R^* as a function of absorber pressure. This is done by fitting data to curves calculated for various combinations of $P'_E V_E(\nu, a_E)$, and X_E .

It should be noted here that the parameters, $P'_A \cdot X_A$ and $V_A(\nu, a_A)$ are known either from measurement in this experiment, i.e., by measuring X , or from CO absorption measurements reported by other workers [7].

The Voigt function is given in terms of an integral whose solution is obtained by various approximation methods, each one effective for a limited range of values of a (see chap. 4 of reference [1]). Therefore, no attempt has been made to derive a general relationship between the measured quantity R^* and the line shape parameter of interest a_E such as exists between W , the equivalent width, and γ_c in the case of the Ladenburg-Reiche curve of growth formulation. Since the absorber pressure is varied over a wide range (0-600 torr) in this experiment, the value of a_A is changed with

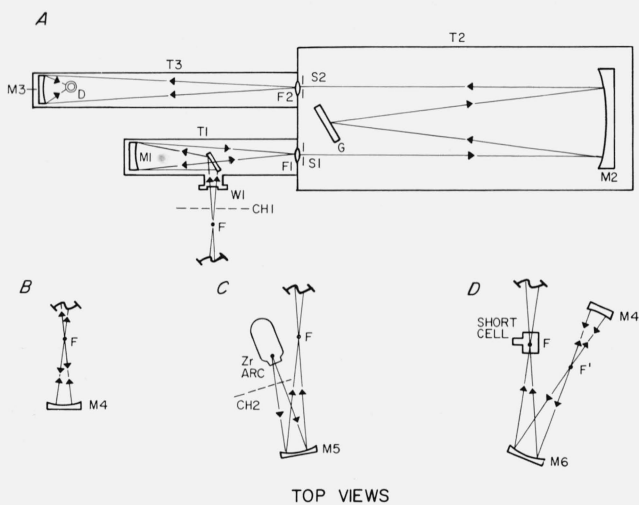


FIGURE 1. *Experimental apparatus.*

each measurement. A computer program is used to evaluate R^*/R^0 for various experimentally realized conditions (absorber path length and pressure, etc.). These calculations are then compared directly with experimental determinations of the same quantity on plots of R^* versus absorber pressure. The quantities a_E and $P'_E \cdot X_E$ determine a particular curve in a family of calculated curves for R^* . The curve that best fits the experimental data determines the values of $P'_E \cdot X_E$ and a_E for a particular line. Additionally, X_E should be the same for all lines in the flame and P'_E can be calculated knowing the line strength, temperature and pressure.

2. Experimental Apparatus and Procedure

The hot CO source used in this study was a commercial welding torch with a No. 3 burner tip having an orifice of 15 mm. A slightly fuel-rich mixture of acetylene and oxygen was burned in air. The gas flow rates were 0.29 liter/s acetylene and 0.33 liter/s oxygen. The rates were determined by flowmeters placed between the gas cylinders and the torch assembly. Commercial welding grade gases were used.

The outer luminous envelope of the oxygen-acetylene flame immediately above the inner luminous cone was focused on the spectrometer slit. The diameter of this outer envelope was approximately 7 mm. The flame was tilted slightly from the vertical so that the image formed at the instrument entrance slit S1 (see figure 1-A) lies along that portion of the curved slit arc which is behind the field lens F1. The spectrometer is housed in three separately evacuable tanks T1, T2, and T3. T1, which houses the entrance slit illuminating optics, affords an absorption path of 113.76 cm when used as an absorption cell. In addition, short cells of 1.005 and 9.72 cm were used for some of the measurements. They were connected to the vacuum system and placed at the focus F as shown in section D of figure 1.

Absorption cell pressures were read on a mercury manometer using a long-focus traveling microscope.

The meniscus on the mercury column was read to 0.01 mm with a reproducibility of two successive readings of approximately 0.05 mm. Atmospheric pressure changes were monitored on a separate closed manometer.

The instrument used in this work was a 1.83 meter Ebert-Fastie monochromator [8]. A replica grating 152 mm high \times 202 mm wide ruled 295 lines/mm and blazed at 4.0 μ m was used. The instrument has a theoretical resolving power of 51,500 in the first order.

The optical components of the instrument are shown in figure 1-A. M1 is a 114 mm diam 650 mm radius of curvature spherical mirror. W1 is a calcium fluoride window; F1 is a field lens of the same material which images mirror M1 onto M2. The source may be either placed or focused at point F in figure 1. The light from the source is then imaged by mirror M1 onto slit S1. The slit assembly is of the curved, proving-ring design [8]; the entrance and exit slits lie on the same 216 mm diam circle. Mirror M3 is an on-axis ellipsoid having focal foci of 1140 mm and 64.5 mm and forms a 15:1 reduced image of S2 onto the detector. The detector D is an indium antimonide photovoltaic cell cooled with liquid nitrogen. The detector has a D^* (500; 900; 1) of 20.4×10^9 and an impedance of 10 k Ω . The wavelength scan is accomplished by means of a twelve-speed reversible, motor-driven gearbox actuating a "sine-drive" mechanism [9].

Lines in the fundamental region of the carbon monoxide spectrum were used as calibration standards, the entire spectrum being scanned and the differences between measured and calculated wavelength values plotted. The shape of this error curve was used to determine the required adjustments to the sine drive mechanism [10]. A wavenumber calibration of the spectrometer scan was then obtained using the known positions of CO lines in the regions of interest. The radiation incident upon the detector is interrupted at 450 Hz by a mechanical chopper (CH1 in fig. 1) and produces an a-c signal at the detector. A phase-sensitive amplification system is used and the output is displayed on a strip chart recorder. The linearity of the detector and amplifier system was checked by a set of neutral density filters constructed and calibrated in this laboratory. The recorder deflection was proportional to the input signal to within 1 percent.

The CO emission spectrum was studied in detail in two regions of interest, namely, in the vicinity of $P_{21} 1-0$ at 2055 cm^{-1} to $P_{17} 1-0$ at 2073 cm^{-1} and $R_{23} 1-0$ at 2224 cm^{-1} to $R_{32} 1-0$ at 2249 cm^{-1} . In order to determine flame temperature scans of the R branch of the 1-0 band were made; a typical spectrum is shown in figure 2. The rotational and vibrational temperature estimates were obtained from such spectra. The heights of the various lines were measured, reduced by the appropriate transition probabilities, etc., and plotted versus the upper state energy. The results are shown in figure 3.

For the determination of the absorption coefficients at the line centers scans at 1 $\text{\AA}/\text{min}$ were taken across unblended 1-0 and 2-1 lines on either side of $P_{18} 1-0$ and $R_{28} 1-0$. The scans were made without mirror M4 (Fig. 1-B) behind the flame and then repeated with the

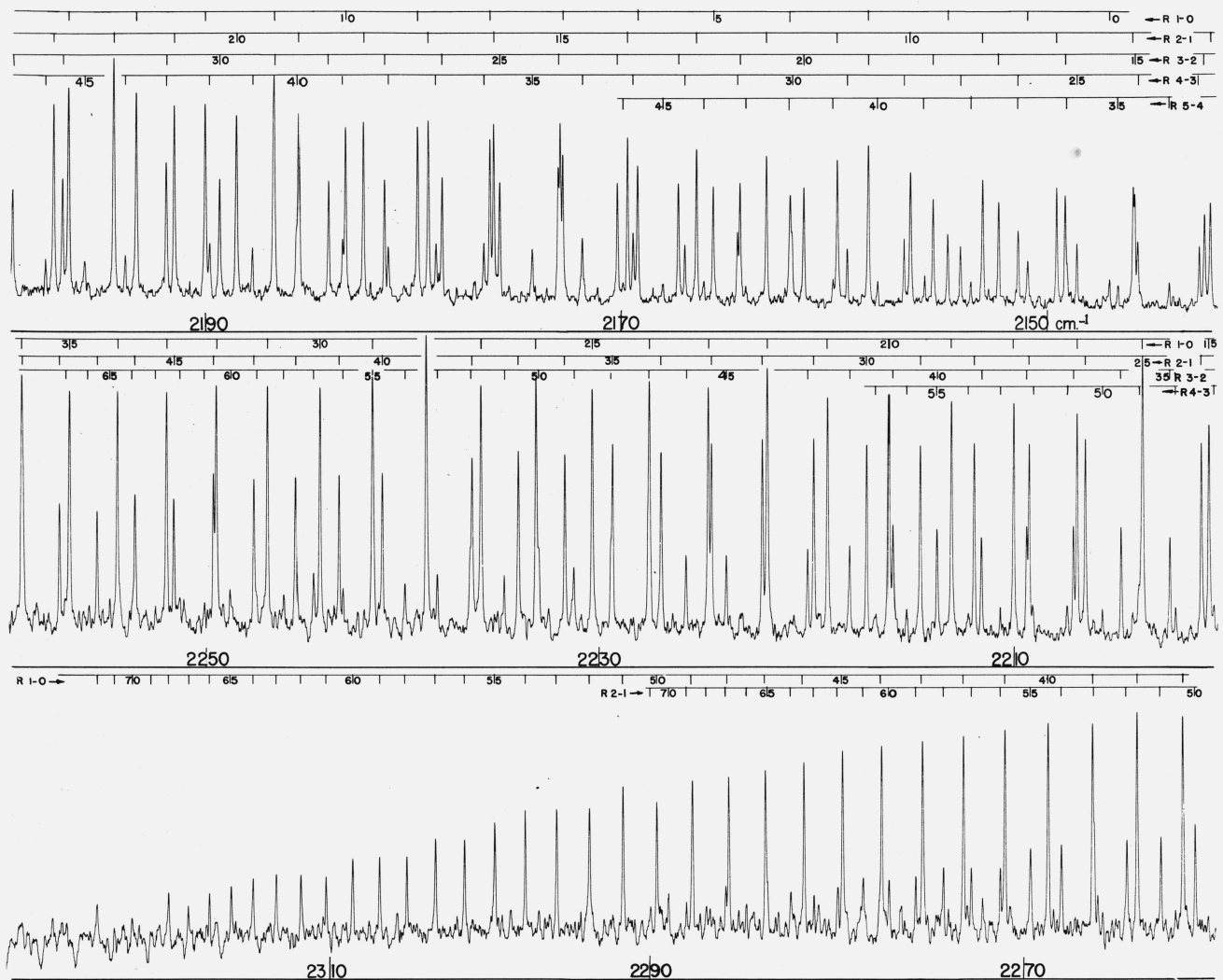


FIGURE 2. R Branch emission.

mirror in place. The ratio of integrated emissivity for the two arrangements was 0.50 ± 1 percent as measured on R₅ 4-3 at 2085.739 cm^{-1} . For each of the lines measured, this ratio R_{L1}/R_{L2} was compared to the family of computed curves of R_{L1}/R_{L2} (a) versus $P'X$. For a chosen value of a , the measured value of (R_{L1}/R_{L2}) in conjunction with figure 4 should determine $P'X$ for a particular line. This procedure is described in more detail in section 3.2.

Integrated absorptivity measurements were made using the arrangement illustrated in section C of figure 1. By Kirchoff's law this measurement gives the integrated emissivity of the lines. Radiation from a Zr arc lamp fitted with a sapphire window was interrupted by a second 450 Hz chopper CH2. Mirror M5 formed an image of the lamp at F, the focus of the instrument entrance mirror. With the chopper CH1 turned off and CH2 running, only the emission from the Zr lamp was modulated at 450 Hz and recorded. No emission from the flame itself was recorded.

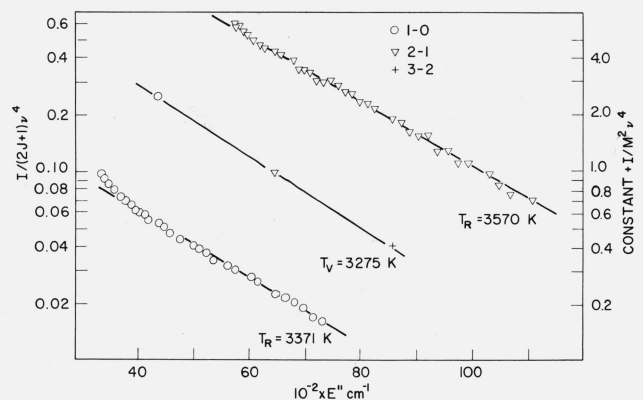


FIGURE 3. Log intensity versus upper state energy E'' .

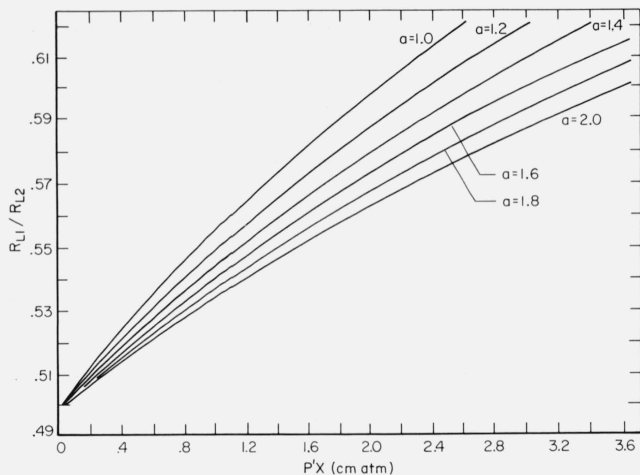


FIGURE 4. R_{l1}/R_{l2} Computed as a function of $P'X$ for various values of a .

The second step in the determination of a_E involves the reabsorption of the flame emission lines by room temperature CO. The experimental arrangements of either section B or D of figure 1 were used for these measurements. An adjacent line from a hotter band was used as a consistent wave number reference for each scan. A line was scanned initially at zero absorber pressure and subsequently with various pressures in the absorption cell. Pressure readings were made before and after each scan. The maximum observed variation in any two readings was less than 0.1 torr.

The recorded traces were photocopied and the line areas determined by weighing the shape cut out of the copy. This procedure was determined to be satisfactorily reproducible, the maximum observed deviation from an average of 14 trials being 5 percent.

3. Results

3.1. Preliminary Calculations

A calculation of energy levels and line positions for the fundamental and first overtone vibration-rotation bands ($\Delta v = 1$, $\Delta v = 2$) of CO has been carried out using a Dunham potential [11] as modified by Woolley [12]. The constants were taken from Goldberg and Mueller [13, 14]. These calculations were used for identification of CO emission lines in the fundamental region. Lines were observed up to the 6-5 vibrational band and for J values as high as 72 in the 1-0 band.

A computer program for calculating Voigt functions has been devised by E. C. Young [15, 16]. An adaptation of this code was used as a subroutine in a larger program to calculate integrated emissivities.

The line strengths used were derived from the calculations of L. A. Young [17, 18]. The line strength S_l^u for a given line can be written in terms of the band strength a_n as follows:

$$S_l^u = a_n \frac{e^{-E_l/kT}}{Q} \left| m \right| \frac{\nu_{ul}}{\nu_0} [1 - \exp(-hc\nu_0/kT)] \quad (11)$$

where E_l is the lower state energy and Q is the partition function at the temperature T , summed over all states of the molecule, m is the rotational index, ν_{ul} is the wavenumber of the transition, and ν_0 is the wavenumber of the band center.

The band strength a_n is given by

$$a_n = \frac{8\pi^3\nu_0}{3hc} L_0 |R_{v''}^{v'}(m)|^2 \quad (12)$$

where L_0 is Loschmidt's number ($2.69 \times 10^{19} \text{ cm}^{-3} \text{ amagat}^{-1}$), and $R_{v''}^{v'}(m)$ is the matrix element between the upper (v'') and lower (v') vibrational states which has a slight m dependence for a given $v'' \rightarrow v'$ transition. The rotational dependence of $R_{v''}^{v'}(m)$ is given by the Herman-Wallis [19] F factor:

$$|R_{v''}^{v'}(m)|^2 = |R_{v''}^{v'}|^2 F_n^{v''}(m). \quad (13)$$

The vibrational dependence of $R_{v''}^{v'}(m)$ for the case of a linear dipole moment and a Morse potential is given by the binomial coefficient:

$$|R_{v''}^{v'}|^2 / |R_0^{v''}|^2 = \frac{(v+n)!}{v!n!} \quad (14)$$

for small v . Young's [17] calculations were used for numerical values of $R_0^{v''}$ and $F(m)$. These calculations also show that eq (14) is correct to within 0.2 percent for $n=1$ and $v \leq 2$. The calculated values of partition functions and line strengths for selected lines at different temperatures are given in table 1.

The machine computation of equivalent width for a selected line, $P_{20} 1-0$, was compared with analytic expressions both in the linear and square root regions of the curve-of-growth.

TABLE 1. Calculated values of the partition function and line strength for various CO lines at different temperatures

Temp (K)	273.16	300	3500
Q	99.0731	108.773	2186.005
1-0 LINE	$S (\text{cm}^{-2}\text{amgt}^{-1})$	$S (\text{cm}^{-2}\text{amgt}^{-1})$	$S (\text{cm}^{-2}\text{amgt}^{-1})$
P 20	0.730	0.886	$7.407 \cdot 10^{-2}$
P 18	1.451	1.640	$7.139 \cdot 10^{-2}$
P 16	2.628	2.788	$6.73 \cdot 10^{-2}$
R 25	$9.943 \cdot 10^{-2}$	0.148	$9.014 \cdot 10^{-2}$
R 28	$2.174 \cdot 10^{-2}$	$3.756 \cdot 10^{-2}$	$8.905 \cdot 10^{-2}$
R 31	$3.931 \cdot 10^{-3}$	$7.986 \cdot 10^{-3}$	$8.580 \cdot 10^{-2}$
Temp (K)	300		3500
Q	108.773		2186.005
2-1 LINE	$S (\text{cm}^{-2}\text{amgt}^{-1})$		$S (\text{cm}^{-2}\text{amgt}^{-1})$
P 14	2.988×10^{-4}		$4.892 \cdot 10^{-2}$
P 12	4.210×10^{-4}		$4.416 \cdot 10^{-2}$
P 10	3.361×10^{-4}		$3.850 \cdot 10^{-2}$
R 36	3.103×10^{-8}		$6.375 \cdot 10^{-2}$
R 39	4.310×10^{-9}		$5.815 \cdot 10^{-2}$
R 42	5.028×10^{-10}		$5.201 \cdot 10^{-2}$

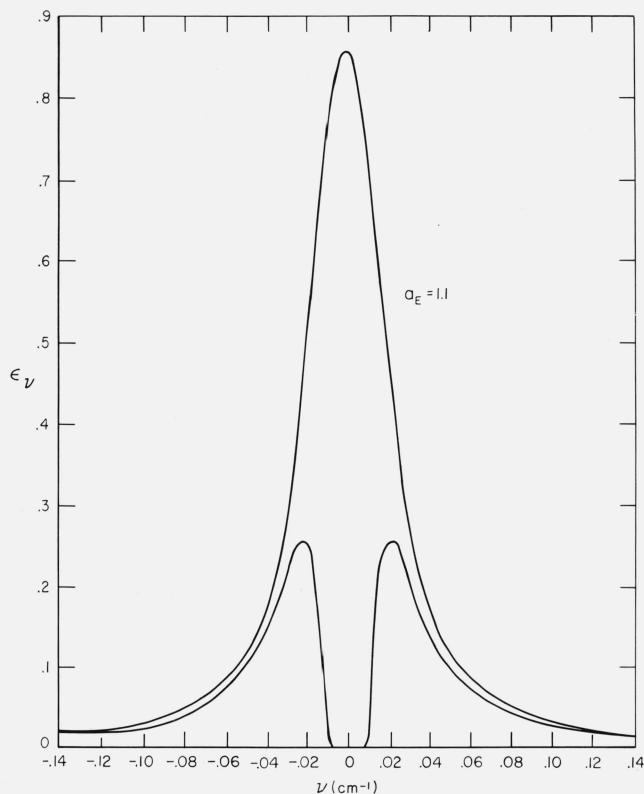


FIGURE 5. Calculated profile for $P_{20} 1-0$ (emission) for $a_E = 1.1$ and $P'_E X_E = 2.4$.

Upper curve—No absorber. Lower curve absorber of 9.8 torr, 113.8 cm path.

At a pressure of 0.5 torr, the line is in the linear region and is predominantly Doppler shaped; its equivalent width is given by Penner [1] as:

$$W_D = \sum_0^{\infty} \frac{SX (-PX)^n}{(n+1)! \sqrt{n+1}} \quad (15)$$

At the above pressure and a path length of 113.8 cm the machine calculation gives $\bar{W} = 4.1018 \times 10^{-3} \text{ cm}^{-1}$ for $P_{20} 1-0$. This differs by 0.08 percent from the value calculated using eq (15). The machine calculation was checked in the square root region of the curve of growth, where the equivalent width is given by [20]:

$$\bar{W} = 2(s^0 \gamma^0 l)^{1/2} (1 - \pi(l^0/W^0)^2 + \dots) \quad (16)$$

where $W^0 = \bar{W}/P$. Table 2 shows the results for the same absorber path, 113.8 cm, and a pressure of 50 torr.

As can be seen in table 2 it is necessary to include the wing contributions over a large distance from the line center in order to get good agreement between the two calculations. The program was formulated in such a way that R^* could be calculated for various lines and absorber pressures by inserting as input: emission line position and strength, flame temperature, absorber pressure and temperature, and path length. Figure 5 shows the resultant line profile computed for $P_{20} 1-0$

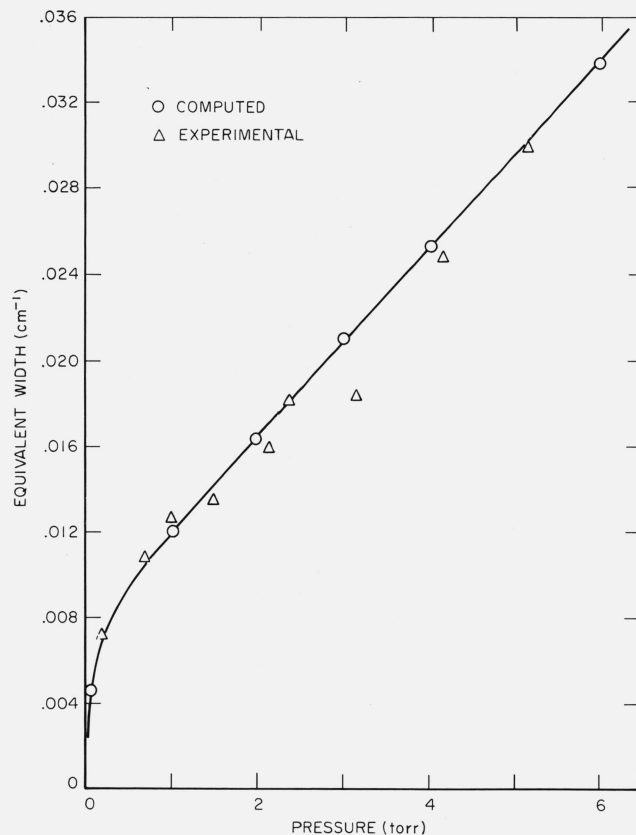


FIGURE 6. Calculated and measured equivalent width for $P_{20} 1-0$ versus pressure.

in emission for the two cases: (1) no CO in the 113.8 cm absorption cell and, (2) a pressure of 9.8 torr.

The equivalent width of $P_{20} 1-0$ versus pressure was then measured in absorption at room temperature. These measurements were used to check the agreement between computer calculations for \bar{W} and actual laboratory measurements. Figure 6 is a graph of these results.

3.2. Experimental Results

Temperature Determination. Figure 2 is a typical recording of the CO emission spectrum in the R branch. A temperature determination is shown in figure 3 where the quantity $\log(I/(2J+1)\nu^4)$ is plotted against the upper state energy E'' . The slopes of the lines for each band indicate that there is approximate thermal equilibrium among the various rotational levels in the upper

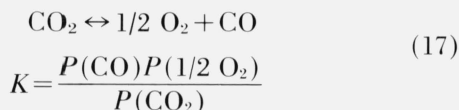
TABLE 2. Contributions to $\bar{W}_{P_{20} 1-0}$ at 50 torr for various distances from line center

cm^{-1}	W Program cm^{-1}	W Formula cm^{-1}	Difference
0 - 0.3	0.231081		
0.3 - 10	.026972		
1.0 - 10	.010941		
10 - 100	.001096		
0 - 100	.27009	0.27151	-0.52 percent

state and that one can estimate an effective rotational temperature from the data. The rotational temperatures T_R are found to be 3570 K for the 2-1 band and 3371 K for the 1-0 band (excluding the initial part of the curve). The vibrational temperature T_V for R_{23} is found to be 3275 K. This is in agreement with earlier work which indicates that lower temperatures are usually observed for the vibrational mode than for the rotational mode in such flames [21] near the reaction zone.

Since there is some atmospheric CO_2 absorption for wavenumbers greater than 2300 cm^{-1} , the apparent intensity data for some of the 1-0 lines in this region will be less than their true intensity. In addition, there is evidence of self-absorption in the strongest 1-0 lines as shown in figure 3. Accordingly, data were heavily weighted in favor of the 2-1 band in choosing the value of 3500 K for T_R ; no correction was needed for self-absorption.

The calculated equilibrium temperature for $\text{C}_2\text{H}_2\text{-O}_2$ flame in which the fuel-oxygen ratio is twice that of a stoichiometric mixture is 3400 K [22]. The equilibrium constant K for the reaction:



as given by Gaydon [23], is 0.34 at 3000 K and 1.58 at 3500 K. Therefore, one would expect little undissociated CO_2 at 3500 K. Indeed very little CO_2 emission was observed from the flame, which supports the estimate of 3500 K.

$P'X$ and a may be determined for a particular emission line by taking the quotient of its integrated intensity for two path lengths. If a mirror is placed behind the emitting volume doubling the path for the second measurement, then the ratio of integrated intensities should be

$$\frac{R_{L1}}{R_{L2}} = \frac{\int_{\Delta\nu} \left[1 - \exp(-P' \cdot X \cdot V(a, \nu)) \right] d\nu}{\int_{\Delta\nu} \left[1 - \exp(-P' \cdot 2X \cdot V(a, \nu)) \right] d\nu} \quad (18)$$

$P'X$ can be determined for a chosen value of a by comparing the two path measurements with the values calculated using the above expression. Penner [1] has calculated the above ratio for a Voigt line shape $V(\nu, a)$ and for values of $P'X$ and a which we can expect to encounter for CO at 3500 K.

Trial calculations of expression (18) using the previously described program demonstrated that the calculated ratio depends upon the interval $\Delta\nu$ over which the integration is carried out since small but finite contributions to (18) occur at large distances from the line center for $a > 1$.

In order to correspond to our measured values, a family of curves of R_{L1}/R_{L2} ($P'X$) was computed for various values of a . The integrations were carried out for the range of $\Delta\nu$ for which the emissivity $\epsilon > 0.01$.

This criterion depends upon the fact that consistent measurements could be made for recorder deflections ≥ 1 percent of full scale.

The measured values of R_{L1}/R_{L2} are shown in column 4 of table 3. Corresponding values of $P'X$ are shown for $a = 1.0$ and 1.4. Column 7 of table 3 lists values of P' calculated from eq (3).

The integrated emissivity for individual lines was determined from absorption measurements, as previously described. Figure 7-A shows the recorder tracing for such measurements on P_{20} 1-0, P_{14} 2-1 and P_8 3-2. In B and C of figure 7 are traces of R_{L1} and R_{L2} respectively for each of these lines. A total of four runs was used to determine the ratio R_{L1}/R_{L2} for each line. This ratio was used to correct the experimental values of the integrated emissivity for each line measured with the absorber in the path, since these measurements were made with the mirror behind the flame. Table 3 contains the experimentally determined values of $R_{L1} = \int \epsilon(\nu) d\nu$ and R_{L1}/R_{L2} for each of the lines investigated.

In addition to the measurement of R^* for isolated 1-0 emission lines, studies were also made of two overlapped pairs of 1-0 and 2-1 lines, namely, P_{18} (1-0)- P_{12} (2-1) and R_{28} (1-0)- R_{39} (2-1). R^* was measured for these near coincident pairs in the normal manner. The R^* computed to represent the data then took the form

$$R^* = \int_{\Delta\nu' + \Delta\nu''} \left\{ 1 - \exp \left[-P'_{E'} X_{E'} V_{E'}(\nu, a_{E'}) \right] - P'_{E''} X_{E''} V_{E''}(\nu, a_{E''}) \right\} \left\{ \exp \left[-P'_{A'} X_{A'} V_{A'}(\nu, a_{A'}) \right] \right\} d\nu \quad (19)$$

where E' refers to the 1-0 emission line, E'' to the 2-1 emission line, and A' to the 1-0 absorption line.

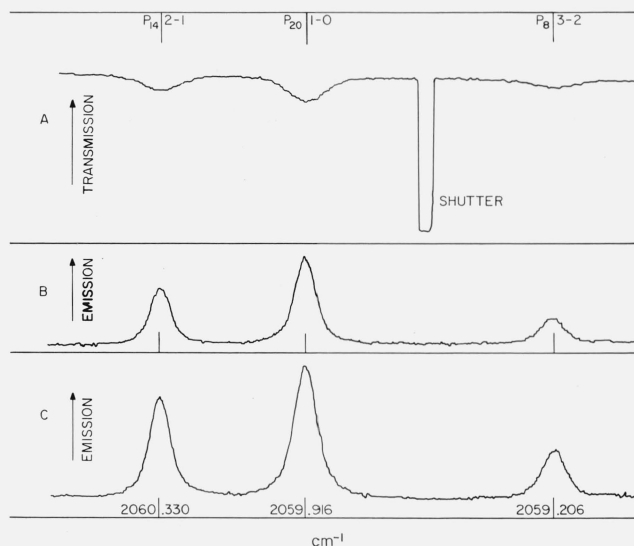


FIGURE 7. Spectra of P_{20} 1-0, P_{14} 2-1, and P_8 3-2. A—Absorption, B—emission, C—emission with mirror behind flame.

TABLE 3. Experimental values of RL1, RL1/RL2, and $P'X$ and calculated value of P' for various CO lines at $P = 1 \text{ atm}$ and $T = 3500 \text{ K}$

Line	Position in cm^{-1}	RL1	RL1/RL2	$P'X^*$ for $a = 1.0$	$P'X^*$ for $a = 1.4$	P' calculated
P 16 1-0	2077.651	$0.027 \pm 1\%$	0.603	2.16	2.80	3.82
P 10 2-1	2077.137	$.0186 \pm 2.6\%$.539	0.66	1.20	1.12
P 18 1-0	2068.849	$.0441 \pm 1.6\%$				4.04
P 12 2-1	2068.800					
P 20 1-0	2059.916	$.0306 \pm .8\%$.591	1.84	2.40	4.09
P 14 2-1	2060.330	$.0202 \pm 2\%$.544	0.76	1.00	1.45
R 25 1-0	2230.525	$.0341 \pm 1.1\%$.572	1.26	1.80	4.74
R 36 2-1	2231.915	$.0193 \pm 1.8\%$.540	0.69	0.91	1.65
R 28 1-0	2238.952	$.0515 \pm .8\%$				4.66
R 39 2-1	2238.924					
R 31 1-0	2247.027	$.0307 \pm 2.7\%$.592	1.86	2.42	4.49
R 42 2-1	2245.566	$.0212 \pm .7\%$.511	0.19	0.28	1.34

* Values obtained by using graph in Figure 4.

Typical spectra are shown in figures 8 and 9. Figure 8 shows $P_{20} 1-0$ and $P_{14} 2-1$ (here the 1-0 line is isolated). The full upper trace is $R_{1,2}$ for no absorber, the lower trace is $R_{1,2}^*$ for an absorber of 9.8 torr CO and a path of 113.76 cm at 300 K. Figure 9 shows the blend of $P_{18} 1-0$ and $P_{12} 2-1$ under the same two absorber conditions. The computed profile of P_{20} under these conditions appears in figure 5. The profile computed for the $P_{18} (1-0) - P_{12} (2-1)$ blend is shown in figure 10. Figure 11 shows experimental and computed values of R^* versus absorber pressure compared for $P_{16} 1-0$. Results for all other lines studied were obtained from similar plots.

In most cases, measurements were made at two absorber path lengths for each of the lines. The values of a_E and $P'_E X_E$ determined for a given emission line were averaged if the two determinations yielded differing values.

The averaged values of a_E and $P'X$ obtained experimentally are listed in table 4. Also listed are the values of $P'X$ calculated according to eq (3), using appropriate line strengths and a value of X determined by the flame thickness. The flame diameter was $7.0 \text{ mm} \pm 8 \text{ percent}$. This gives an experimental value for the equilibrium

concentration of CO at 3500 K of 71 percent, and a value of $X = 0.5 \text{ cm atm}$. Such a high concentration of CO in a fuel rich $\text{C}_2\text{H}_2 - \text{O}_2$ flame at 3500 K does appear consistent with previous estimates [23].

The fitting of curves such as those shown in figure 11 at zero absorber pressure was primarily controlled by the choice of $P'_E X_E$ while the remainder of the curve was fitted by the proper choice of a_E . The results collected in table 4 show that although the sensitivity of the data to trial values of $P'_E X_E$ and a_E is less than one might desire, fairly consistent values have been found. Values of $P'_E X_E$ and a_E were altered until the calculated emissivity agreed with measurement to within 2 percent for zero absorber pressure. Points were then calculated for two or three absorber pressures to determine whether or not the selected combination of $P'_E X_E$ and a_E would fit the entire curve of R^* versus absorber pressure.

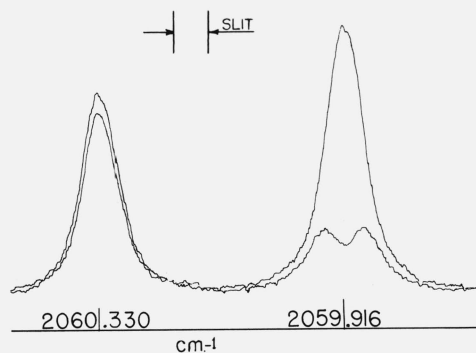


FIGURE 8. Spectra of $P_{20} 1-0$ and $P_{14} 2-1$.

Upper curve—no absorber. Lower curve—absorber of 9.8 torr, 113.8 cm path.

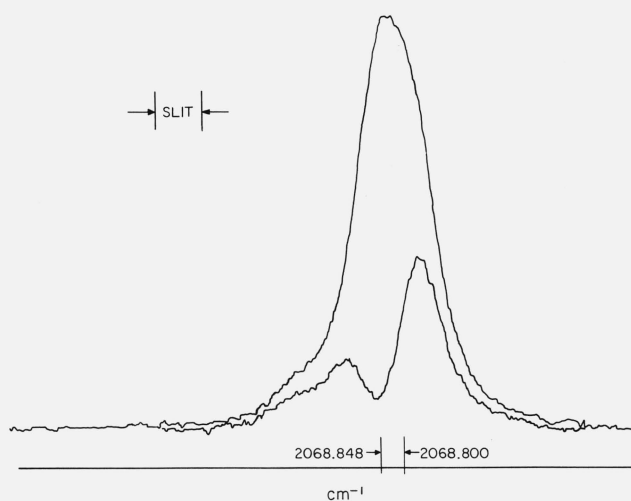


FIGURE 9. Spectra of $P_{18} 1-0$ and $P_{12} 2-1$.

Upper curve—no absorber. Lower curve—absorber of 9.8 torr, 113.8 cm path.

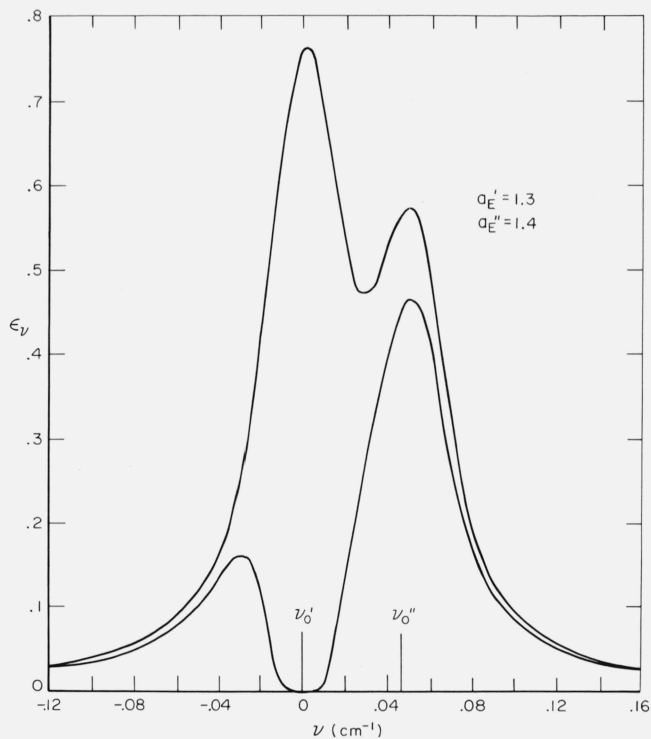


FIGURE 10. Computed profile of P₁₈ 1-0 and P₁₂ 2-1 blend in emission for $a_E' = 1.3$, $P_E'X_E' = 1.9$; $a_E'' = 1.4$; $P_E''X_E'' = 1.1$. $\nu_0' = \nu_0'' = 0.048 \text{ cm}^{-1}$. Upper curve—no absorber. Lower curve—absorber of 9.8 torr, 113.8 cm path.

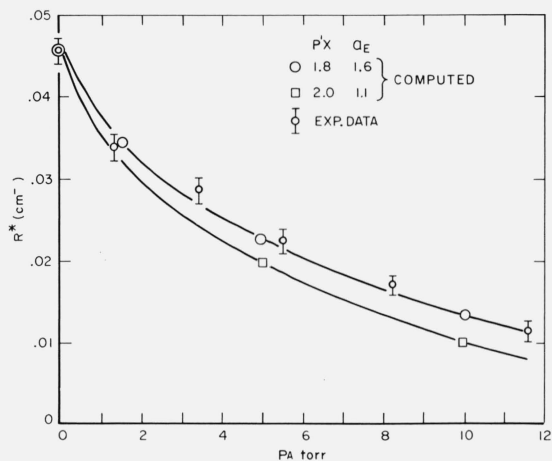


FIGURE 11. R^* for P₁₆ 1-0 for 113.8 cm path.

For a fixed value of $P_E'X_E'$, this analysis was sensitive to a 10 percent change in a_E . For zero absorber pressure, the calculated emissivity was sensitive to a 5 percent change in $P_E'X_E'$ and a 25 percent change in a_E . The analysis of the two combinations including (1-0)-(2-1) blends was still less sensitive to changes in the parameters for the 2-1 line. This fact is demonstrated by the 40 percent difference between measurement and calculation for $P_E'X_E'$ for P₁₂ 2-1. However, more reliable values of $P_E'X_E'$ were obtained using the above procedure than by the two path method previously described. The comparison of experiment to calculations of R_{L1} rather than the ratio R_{L1}/R_{L2} was found to be more sensitive to changes in $P_E'X_E'$ by a

TABLE 4. Experimental results for $P'X$ and a_E at $P = 1 \text{ atm}$ and $T = 3500 \text{ K}$

Line	$P'X$ calculated for $X = 0.50 \text{ cm atm}$	Absorber path in cm	$P'X$ experimental	Average	a_E experimental	Average
P 16 1-0	1.91	113.8 1.005	1.8 1.9	1.85	1.6 1.2	1.4
P 18 1-0	2.02	(113.8 1.005)	1.9 1.9	1.9	1.3 1.3	1.3
P 12 2-1	.64	(113.8 1.005)	1.1 1.1	1.1	1.4 1.4	1.4
P 20 1-0	2.04	*113.8 1.005 113.8	2.2 2.4 2.4	2.33	1.4 1.1 1.1	1.2
R 25 1-0	2.37	9.72	2.4	2.4	1.5	1.5
R 28 1-0	2.33	(113.8 9.72)	2.3 2.3	2.3	1.0 1.0	1.0
R 39 2-1	.76	(113.8 9.72)	0.9 1.0	.95	1.0 1.0	1.0
R 31 1-0	2.24	113.8	1.8	1.8	1.4	1.4

*Indicates no mirror behind flame; linkages indicate line pairs scanned simultaneously.

factor of 4. The principal disadvantage of the two path method is that the observed ratio R_{L1}/R_{L2} for a given value of a is an insensitive function of $P_E^1 X_E$, since the experimental uncertainty in this ratio (about 3%) results in a 20 percent uncertainty in the determination of $P_E^1 X_E$.

4. Discussion

From the experimentally determined values of a_E and the relation $a_E = (\ln 2)^{1/2} \gamma_c / \gamma_D$ one obtains an experimental value for the Lorentz width, γ_c , at 3500 K. It will be recalled that the CO emitter is not in an environment of pure CO, so that γ_c does not correspond precisely to the value for self-broadening. The flame gases are predominantly (~70%) CO, with the remainder mostly H_2 and H; these constituents may be expected to have smaller and greater broadening effects respectively than CO itself.

It is instructive to compare these results to the measurement of Lorentz width at room temperature for pure CO.

The effect of temperature on collision width comes from two factors: the number of collisions (which varies at constant density as $T^{1/2}$ or at constant pressure as $T^{-1/2}$); and the collision diameter, $b_{\text{eff}} = (\sigma_1 \sigma_2)^{1/2}$. The collision diameter is temperature-independent only for the hard-sphere model of the intermolecular potential. Some decrease of b with increasing T is expected for more realistic models which involve the various attractive potentials required to account for the dependence of collision width on m (ref. [24]), the ordinal rotational number.

Moreover, the rotational distribution of colliding molecules is altered at high temperatures in such a way that the resonance effects which lead to a peaking of the width at the most populated J , are considerably reduced. This results in a shift of the width toward higher J .

Our results are presented in figure 12. The right-hand ordinate is the collision diameter; the left-hand ordinate is γ_c^0 (300 K) obtained from the measured value of b_{eff} at 3500 K; i.e. γ_c^0 (300 K) = $a_E \gamma_D \sqrt{3500/300} / \sqrt{\ln 2}$.

For comparison one set of room temperature measurements is also plotted. The solid curve represents the best fit to the room temperature data.

The high-temperature results show only a very slight decrease of b_{eff} with increasing m . This contrasts with the much more rapid decrease, particularly at low m , which is observed at 300 K. However, the average value, 4.2 ± 0.3 Å, is not very different from room-temperature values in the range of m from 12–40, but is definitely higher than the hard-sphere kinetic theory diameter. Interpretation of these facts is uncertain in view of the neglect of the contribution of H_2 and H collisions to the measured b_{eff} . The reduced m -dependence is to be expected from the broader distribution of J -value among colliding molecules. It is worth noting that the expected temperature dependence $\gamma_c \sim PT^{-1/2}$ is verified by comparing measurements taken at 300 K with these at 3500 K. Recent measurements by Hoover and Williams [25] indicate that this dependence is also valid at temperatures as low as 200 K for CO.

The support of the Air Force Cambridge Research Laboratories is gratefully acknowledged. We also wish to thank E. C. Young of the University of Michigan for making available a copy of his program for calculating Voigt profiles, and L. Karr and J. Jalickee for helpful assistance in formulating the other programs used. The help given by W. Pugh and W. Scherer in data collection and reduction is also greatly appreciated.

5. References

- [1] Penner, S. S., Quantitative Molecular Spectroscopy and Gas Emissivities (Addison Wesley Publishing Company, Inc., Reading, Mass., 1959), p. 33, eq (3-34).
- [2] Handbook of Chemistry and Physics, Thirty-Eighth Edition (The Chemical Rubber Company, Cleveland, Ohio), p. 3128.
- [3] Hardy, A. C., and Young, F. M., J. Opt. Soc. Am. **39**, 265 (1949).
- [4] Adel, A., and Barker, E. F., Reviews of Modern Physics **16**, 236 (1944).
- [5] Kostkowski, H. J., and Bass, A. M., J. Opt. Soc. Am. **46**, 1060, (1956).

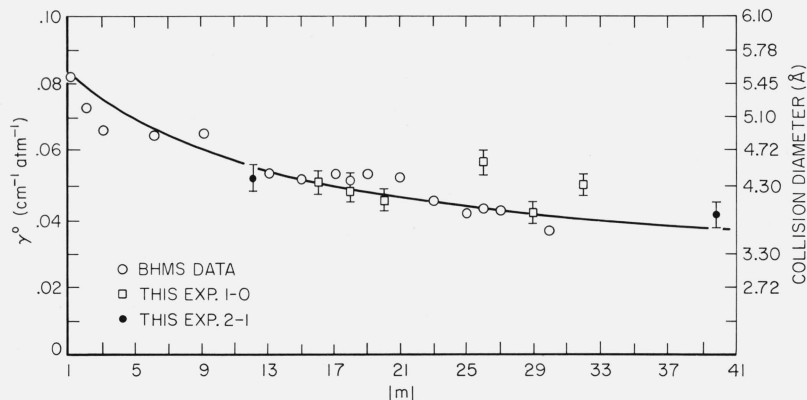


FIGURE 12. Collision width and collision diameter for CO emission lines as a function of m .

- [6] vonPlanta, P. C., *J. Opt. Soc. Am.* **47**, 629 (1957).
- [7] Benedict, W. S., Herman, R., Moore, G. E., and Silverman, S., *Astrophys. J.* **135**, 277 (1962).
- [8] Fastie, W. G., Crosswhite, H. M., and Gloersen, P., *J. Opt. Soc. Am.* **48**, 106 (1958).
- [9] Badger, R. M., Zumwalt, L. R., and Giguère, P. A., *Rev. Sci. Instr.* **19**, 861 (1948).
- [10] Garvin, D., and Weiss, E. L., Informal Report (1965).
- [11] Dunham, J. L., *Phys. Rev.* **41**, 721 (1932).
- [12] Woolley, H. W., *J. Chem. Phys.* **37**, 1307 (1962).
- [13] Goldberg, L., and Mueller, E. A., *Astrophys. J.* **118**, 397 (1953).
- [14] Similar and more recent extensive calculations of CO line positions and intensities at elevated temperatures have recently been made by V. Kunde, NASA Goddard Space Flight Center, see NASA Technical Note TN D-4798 (December 1968), also NASA documents X-622-67-248 (June 1967), and X-622-67-452 (December 1968). See also Jansson, P. A. and Korb, C., *JQSRT* **8**, 1399 (1968).
- [15] Young, E. C., *JQSRT* **5**, 545 (1965).
- [16] Young, E. C., Tables for Calculating the Voigt Profile, Technical Report, University of Michigan (1965).
- [17] Young, L. A., and Eachus, W. J., Avco Everett Research Report 239 (1966) also *J. Chem. Phys.* **44**, 4195 (1966).
- [18] Young, L. A., Avco Everett Research Laboratory, AMP, 188 (1966). Also *JDSRT* **8**, 693, (1968).
- [19] Herman, R., and Wallis, R. F., *J. Chem. Phys.* **22**, 481 (1954).
- [20] Benedict, W. S., Herman, R. C., Moore, G. E., and Silverman, S., *Can. J. Phys.* **34**, 830, 850 (1956).
- [21] Plyler, E. K., Benedict, W. S., and Silverman, S., *J. Chem. Phys.* **20**, 175 (1952).
- [22] Broida, H. P., Energy Transfer in Hot Gases, N.B.S. Circular 523 (1954), page 31.
- [23] Gaydon, A. G. and Wolfhard, H. G., *Flames, Their Structure Radiation and Temperature* 2nd ed. (New York, MacMillan (1960), p. 295.
- [24] Benedict, W. S., and Herman, R., *JQSRT* **3**, 265 (1963).
- [25] Hoover, G. M., and Williams, D., *J. Opt. Soc. Am.* **59**, 28 (1969).

(Paper 75A5-680)